

# CAA: Channelized Axial Attention for Semantic Segmentation

Ye Huang<sup>1</sup> Wenjing Jia<sup>1</sup> Xiangjian He<sup>1</sup> Liu Liu<sup>2</sup> Yuxin Li<sup>3</sup> Dacheng Tao<sup>2</sup>

<sup>1</sup>University of Technology Sydney <sup>2</sup>University of Sydney <sup>3</sup>Byker Biotech Pty Ltd

Ye.Huang-2@student.uts.edu.au

## Abstract

Self-attention and channel attention, modelling the semantic interdependencies in spatial and channel dimensions respectively, have recently been widely used for semantic segmentation. However, computing self-attention and channel attention separately and then fusing them directly can cause conflicting feature representations. In this paper, we propose the Channelized Axial Attention (CAA) to seamlessly integrate channel attention and axial attention with reduced computational complexity. After computing axial attention maps, we propose to channelize the intermediate results obtained from the transposed dot-product so that the channel importance of each axial representation is optimized across the whole receptive field. We further develop grouped vectorization, which allows our model to be run in the very limited GPU memory with a speed comparable with full vectorization. Comparative experiments conducted on multiple benchmark datasets, including Cityscapes, PASCAL Context and COCO-Stuff, demonstrate that our CAA not only requires much less computation resources but also outperforms the state-of-the-art segmentation models based on ResNet-101 on all tested datasets.

## 1. Introduction

Semantic segmentation is a fundamental task in many computer vision applications, which assigns a class label to each pixel in the image. Most of the existing approaches for semantic segmentation (e.g., [2, 3, 29, 27, 9, 16]) have adopted a pipeline similar to the one that is defined by Fully Convolutional Networks (FCNs) [18] and uses fully convolutional layers to output pixel-level segmentation results of the input image, and have achieved state-of-the-art performance. After the FCN approach, there have been many approaches dedicated to extracting enhanced pixel representations from backbone. Earlier approaches, including PSP-Net [32] and DeepLab [4], used a Pyramid Pooling Module (PPM) or an Atrous Spatial Pyramid Pooling (ASPP) module to expand the receptive field and capture multiple-range information to enhance the representation capabilities.

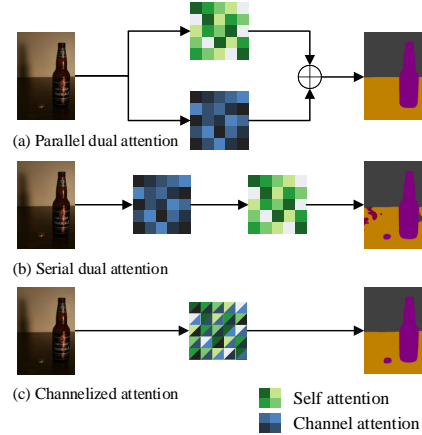


Figure 1. Different dual attention designs

The latest segmentation head researches in recent years mainly focus on using the attention mechanisms to improve the performance. During the early days of attention mechanisms, the Squeeze and Excitation Networks (SENet) [12] introduced a simple yet efficient channel attention module to explicitly model the interdependencies between channels. Meanwhile, the Non-Local Networks [25] proposed self-attention to capture long-range dependencies, so as to produce more correct pixel representations. For each pixel in the feature maps, self-attention makes its representation more similar to the representations of the pixels that are closer, whereas channel attention finds important channels in the entire feature maps and applies different weights back to the extracted features.

To enjoy the advantages of both self-attention and channel attention, some approaches (e.g., [9]) proposed to directly fuse their results with an element-wise addition (as illustrated in Fig. 1(a)). Although they have produced improved performance, the relationship between the contributions of the self-attention and channel attention to the final result is very unclear.

Moreover, calculating two attentions separately not only increases the computational complexity, but also results in

conflicting importance of feature representations. For example, some channels may appear to be important in self-attention for a pixel that belongs to a partial region in the feature maps, but they may be **ignored** by the channel attention, which is calculated by summing up the similarities over the entire feature maps, and hence causing a conflict for semantic classes of a small size. The existing designs (e.g. [26]) combining channel attention and self-attention with a parallel design have similar issues. Channel attention can **ignore** the partial region representation obtained from the overall perspective, which may be required by self-attention. Thus, directly fusing the self-attention results with channel attention results may yield incorrect importance weights for pixel representations.

Attempting to combine the advantages of self-attention and channel attention seamlessly and efficiently, we propose the Channelized Axial Attention (CAA). Specifically, when applying the axial attention maps to the input signal [25], we capture the intermediate results of the dot product before they are summed up along the corresponding axes. Capturing these intermediate results allows channel attention to be integrated for each column and each row, instead of computing on the mean or sum of the features in the entire feature maps. More importantly, when applying the attention maps, we propose a novel transposed approach, which allows the channel attention to be conducted in the whole receptive field. Last but not the least, we develop a novel grouped vectorization approach to maximize the computation speed under limited GPU memory.

In summary, our contributions of this paper include:

- Aiming to integrate self-attention with channel attention effectively and efficiently, we propose a novel Channelized Axial Attention to optimize both the computational complexity and the robustness.
- We re-design the axial attention to enhance the relationship between the attention output and input, and also propose an improved channel attention module to boost the overall performance.
- When applying column and row attention maps, we compute the attention results in a transposed way, which allows the channel attention to be conducted across the whole receptive field.
- We propose a novel grouped vectorization approach to compute the channelized attentions to trade off the computation speed and GPU memory usage, and it is particularly useful when processing large images with limited GPU memory.
- Extensive experiments on three challenging datasets, *i.e.*, PASCAL Context [8], COCO-Stuff [1] and Cityscapes [19], demonstrate the superiority of our approach over the state-of-the-art approaches.

Next, Sect. 2 briefly summarizes the related works. Then, we illustrate the details of our proposed approach in Sect. 3. Sect. 4 presents the experiments and discussion. The paper concludes in Sect. 5.

## 2. Related Works

### 2.1. Capturing Information from Fixed Ranges

The PSPNet [32] proposed a PPM, which used multiple average pooling layers with different sizes together to get average pixel representations in multiple receptive fields, and then upsample and concatenate them together. Similarly, the ASPP in DeepLab [2, 4] used parallel atrous convolutions with different rates to capture information from multiple ranges. The core ideas of both models are to utilize the surrounding information of each pixel in multiple ranges to achieve better pixel representations. Both methods have achieved highest scores in some popular public datasets [8, 19]. However, as claimed in [27], fixed receptive fields may lose important information, to which stacking more receptive fields can be a solution, at the cost of dramatically increased computation.

### 2.2. Attention Mechanisms

**Self Attention.** Non-Local networks [25] introduced the self-attention mechanism to examine the pixel relationship in spatial domain. It usually calculates dot-product similarity or cosine similarity to obtain the similarity measurement between every two pixels in feature maps, and recalculate the feature representation of each pixel according to its similarity with others. Self-attention has successfully addressed the feature map coverage issue of multiple fixed-range approaches [2, 32, 27], but it introduces a huge computation cost due to the full feature map computation. This means that, for each pixel in the feature maps, its attention similarity concerns all other pixels. Recently, many approaches [5, 13, 34, 11] have provided optimized solutions for self-attention. They have not only reduced computation and GPU memory costs but also improved the performance.

**Channel Attention.** Channel attention [12] examined the relationships between channels, and enhanced the important channels so as to improve the performance. SENets [12] conducted a global average pooling to get mean feature representations, and then went through two fully connected layers, where the first one had reduced channels and the second one recovered the original channels, resulting in channel-wise weights according to the importance of channels. In DANet [9], channel-wise relationships were modelled by a 2D attention matrix, similar to the self-attention mechanism except that it computed the attention with a dimension of  $C \times C$  rather than  $H \times W \times H \times W$  ( $C$  denotes the number of channels, and  $H$  and  $W$  denote the height and width of the feature maps, respectively).

### 2.3. Self-Attention + Channel Attention

Combining self-attention and channel attention can provide fully optimized pixel representations in a feature map. However, it is not easy to use their advantages together seamlessly. In DANet [9], the results of the channel attention and self-attention are directly added together. Supposing that there is a pixel belonging to a semantic class that has a tiny region in the feature maps, self-attention can find its similar pixels. However, channel representation of the semantic class with a partial region of the feature maps may not be important in the perspective of entire feature maps, so it may be ignored when conducting channel attention computation. Computing self-attention and channel attention separately (as illustrated in Fig. 1(a)) can cause conflicting results, and thus lower their performance when both results are summarized together. In the cascaded model (see Fig. 1(b)), the channel attention module after the self-attention module may override the result of the self-attention, as channel attention recomputes the channel importance according to the entire feature maps.

Next, we present the details of our proposed CAA approach, which first computes the self-attention row-by-row and column-by-column, and then inserts the channel attention module to integrate both approaches seamlessly.

## 3. Methods

### 3.1. Formulation

Following [25], a 2D self-attention operation in neural networks can be defined by:

$$\mathbf{y}_{i,j} = \sum_{\forall m,n} f(\mathbf{x}_{i,j}, \mathbf{x}_{m,n})g(\mathbf{x}_{m,n}). \quad (1)$$

Here, a pairwise function  $f$  computes the similarity between the pixel representations  $\mathbf{x}_{i,j}$ ,  $\mathbf{x} \in \mathbb{R}^{H \times W \times C}$ , at the position  $(i, j)$  and the pixel representation  $\mathbf{x}_{m,n}$  at all other possible positions  $(m, n)$ , producing a spatial attention map over the whole feature maps. The unary function  $g$  maps the original representation at position  $(m, n)$  to a new domain. In our work, we also take the softmax function as  $f$ , i.e.,

$$f(\mathbf{x}_{i,j}, \mathbf{x}_{m,n}) = \text{softmax}(\theta(\mathbf{x}_{i,j})^T \theta(\mathbf{x}_{m,n})). \quad (2)$$

Thus, given a feature map output from a backbone network such as ResNet [10], the self-attention module firstly uses  $1 \times 1$  convolution  $\theta$  to map the feature maps  $\mathbf{x}$  to a new domain, and then applies dot-product similarity [25] between every two pixels. Then, using this similarity as the weight, Eq. (1) calculates a weighted global sum over all pixels in the feature maps and outputs a new pixel representation  $\mathbf{y}_{i,j}$  at the position  $(i, j)$ .

It can be seen from Eq. (2) that, the original similarity map is of  $H \times W \times H \times W$  dimensions, and is computed as the dot product over the whole feature maps for each pixel. To reduce the computational complexity, we perform axial

attention and calculate weighted pixel representations with our new column and row attention maps, which involve pixels in the same column or row only.

Our axial attention is inspired by the axial transformation [11] but is different from the axial attention in [24], which was calculated in the backbone. Instead, our axial attention is attached to the backbone as an independent module, making it very easy to plug into any other backbone networks to take benefit of their pre-trained weights. Moreover, the calculation of our column and row attention maps is based on the same feature maps, and is beneficial for feature relationship enhancement.

Furthermore, we propose a novel transposed approach to apply the resultant attention maps to the input signal [25], allowing us to integrate the channel attention seamlessly.

Next, we first present the process of computing our new axial attention maps, and then illustrate our transposed approach of applying the axial attention maps transpositionally. Based on this, we present our channelized axial attention, which not only saves the computation cost but also improves the performance at negligible computation cost.

### 3.2. Calculating Axial Attention Maps

In our axial attention, we calculate the attention maps along the column axis and row axis, respectively.

For the  $j$ -th column attention, the attention similarity tensor is calculated by the similarity between the current position  $(i, j)$  and other positions  $(m, j)$  in the  $j$ -th column (instead of all other positions, as in the self-attention), i.e.,

$$A_{\text{col}}(\mathbf{x}_{i,j}, \mathbf{x}_{m,j}) = \text{softmax} \left( \theta(\mathbf{x}_{i,j})^T \theta(\mathbf{x}_{m,j}) \right), \quad j \in [W].^1 \quad (3)$$

Here,  $\theta$  represents the learned feature extraction process for the  $Y$  axis. Each  $A_{\text{col}}(\mathbf{x}_{i,j}, \mathbf{x}_{m,j})$  represents the similarity between  $\mathbf{x}_{i,j}$  and  $\mathbf{x}_{m,j}$  for  $i, m \in [H]$ , so each  $\mathbf{x}_{i,j}$  corresponds to  $H$  column-attention maps  $A_{\text{col}}(\mathbf{x}_{i,j}, \mathbf{x}_{m,j})$ . Thus, the resultant column attention map  $A_{\text{col}}$  is a tensor of  $W \times H \times H$  dimensions.

Similarly, for the  $i$ -th row attention, the similarity attention tensor calculates the similarity between the current position  $(i, j)$  and other positions  $(i, n)$  in the  $i$ -th row, i.e.,

$$A_{\text{row}}(\mathbf{x}_{i,j}, \mathbf{x}_{i,n}) = \text{softmax} \left( \phi(\mathbf{x}_{i,j})^T \phi(\mathbf{x}_{i,n}) \right), \quad i \in [H], \quad (4)$$

where  $\phi$  represents the learned feature extraction process for the  $X$  axis. Similarly, each  $\mathbf{x}_{i,j}$  corresponds to  $W$  row-attention maps  $A_{\text{row}}(\mathbf{x}_{i,j}, \mathbf{x}_{i,n})$ . Thus, the resultant row attention map  $A_{\text{row}}$  is a tensor of  $H \times W \times W$  dimensions.

Thus, instead of calculating an attention map of  $H \times W \times H \times W$  dimensions in self-attention, which has an order complexity of  $\mathcal{O}(H^2W^2)$ , our axial attention computes column and row attention maps and has an order complexity of  $\mathcal{O}(HW)$ .

<sup>1</sup>We use  $i \in [n]$  to denote that  $i$  is generated from  $[n] = \{1, 2, \dots, n\}$ .

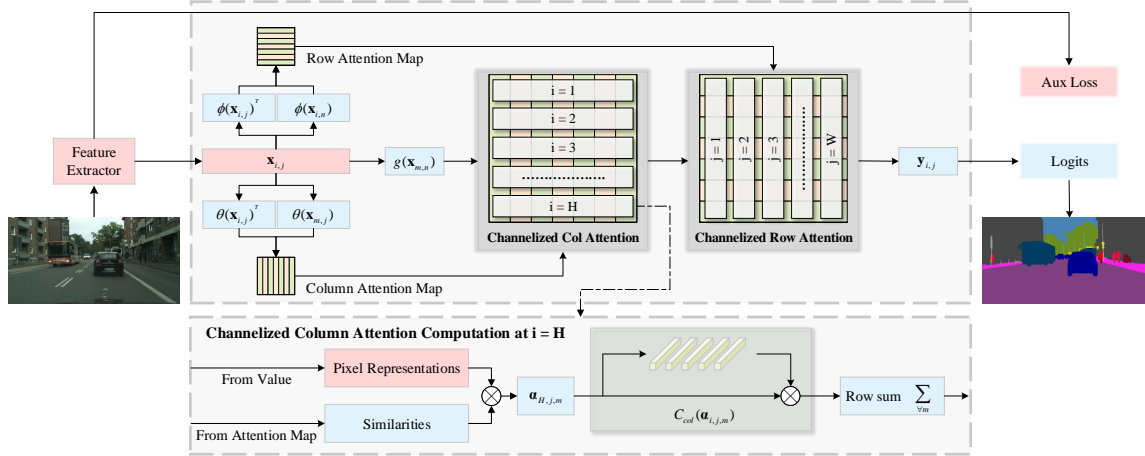


Figure 2. The detailed architecture of our proposed Channelized Axial Attention model. To obtain  $H \times W \times C$  inputs for the channel attention, we apply the resultant column and row attentions in a transposed way. The bottom section illustrates the channelization of the column attention for  $i = H$ .

It is worth of pointing out that, in Eqs. (3) and (4), the calculations of our column and row attention maps both use the same feature  $\mathbf{x}_{i,j}$  extracted from the backbone module as the input, as shown in Fig. 2. This is different from [24], where the row attention map was computed based on the result of the column attention. By using the same feature as the input, the dependency of the final output  $y_{i,j}$  on the feature  $\mathbf{x}_{i,j}$  has been enhanced effectively, instead of using the skip connection as in [24].

### 3.3. Applying Axial Attention Transpositionally

With the column and row attention maps  $A_{\text{col}}$  and  $A_{\text{row}}$ , the final value weighted by the column and row attention maps can be represented as:

$$y_{i,j} = \sum_{\forall n} \left( A_{\text{row}}(\mathbf{x}_{i,j}, \mathbf{x}_{i,n}) \left( \sum_{\forall m} A_{\text{col}}(\mathbf{x}_{i,j}, \mathbf{x}_{m,j}) g(\mathbf{x}_{m,n}) \right) \right) \quad (5)$$

For the convenience of illustration, we introduce two variables  $\alpha_{i,j,m}$  and  $\beta_{i,j,n}$  to capture the intermediate, weighted features by column and row attention maps, respectively, where

$$\alpha_{i,j,m} = A_{\text{col}}(\mathbf{x}_{i,j}, \mathbf{x}_{m,j}) g(\mathbf{x}_{m,j}) \quad (6)$$

and

$$\beta_{i,j,n} = A_{\text{row}}(\mathbf{x}_{i,j}, \mathbf{x}_{i,n}) \sum_{\forall m} \alpha_{i,j,m}. \quad (7)$$

As illustrated later in Sect. 3.4, capturing the intermediate attention results brings opportunity to conduct independent channel attentions for each partial attention result.

Thus, Eq. (5) can be simplified to:

$$y_{i,j} = \sum_{\forall n} \beta_{i,j,n} = \sum_{\forall n} A_{\text{row}}(\mathbf{x}_{i,j}, \mathbf{x}_{i,n}) \left( \sum_{\forall m} \alpha_{i,j,m} \right). \quad (8)$$

The above Eqs. (6), (7) and (8) show that, the computation of the dot product is composed of two steps. 1) The

element-wise multiplication for applying the column attention as shown in Eq. (6) and applying the row attention as shown in Eq. (7) for column and row attentions, respectively; 2) The summarization of the elements along each row and column according to Eq. (8).

Also note that, the element-wise computation shown in Eqs. (6) and (7) indicates that we apply the column and row attention maps in a transposed way. That is to say, the column and row attention results are decomposed along the transposed axis (*i.e.*, decomposing  $\alpha_{i,j,m}$  along the row direction and  $\beta_{i,j,n}$  along the column direction), instead of along the column and row, into multiple 3-dimension column or row attention results for different  $i$  or  $j$ . This is illustrated in Fig. 2.

This transpositional way of applying the axial attentions not only produces partial column and row attention results with consistent dimensions, but also enables them to capture the dependencies inherent in the other axis so as to conduct channelization in the whole receptive field.

### 3.4. Channelized Axial Attention

As stated earlier in Sect. 1, computing self-attention and channel attention separately and then fusing them together directly can cause conflicting feature representations. This means, important channels for a class with a small area in the feature maps can be dominated and therefore ignored in the computation of the global channel attention. Ideally, the computation of the self-attention for each channel also needs its own channel attention computation. To realize this, we propose a novel *Channelized Axial Attention*, which mainly relies on the intermediate results in Eqs. (6) and (7) with our novel transposed computation.

After we have the intermediate results  $\alpha_{i,j,m}$  and  $\beta_{i,j,n}$



in Eqs. (6), (7) and (8), we now introduce our channelized attentions  $C_{\text{col}}$  and  $C_{\text{row}}$ , corresponding to the column attention and row attention, respectively, as:

$$C_{\text{col}}(\alpha_{i,j,m}) = \text{Sigmoid} \left( \text{ReLU} \left( \frac{\sum_{\forall m,j} (\alpha_{i,j,m})}{H \times W} \omega_{c1} \right) \omega_{c2} \right) \alpha_{i,j,m} \quad (9)$$

and

$$C_{\text{row}}(\beta_{i,j,n}) = \text{Sigmoid} \left( \text{ReLU} \left( \frac{\sum_{\forall i,n} (\beta_{i,j,n})}{H \times W} \omega_{r1} \right) \omega_{r2} \right) \beta_{i,j,n} \quad (10)$$

where  $\omega_{c1}$ ,  $\omega_{c2}$ ,  $\omega_{r1}$  and  $\omega_{r2}$  represent the learnable relationships between different channels in  $\alpha_{i,j,m}$  and  $\beta_{i,j,n}$ , which will be discussed later in Sect. 3.6.

Thus, instead of directly using  $\alpha_{i,j,m}$  and  $\beta_{i,j,n}$  as in Eq. (8), for each column and row, we obtain the seamlessly mixed attention results for spatial channels, where the intermediate results  $\alpha_{i,j,m}$  and  $\beta_{i,j,n}$  are weighted by the channelized axial attention defined in Eqs. (9) and (10) as:

$$y_{i,j} = \sum_{\forall n} C_{\text{row}} \left( A_{\text{row}}(x_{i,j}, x_{i,n}) \left( \sum_{\forall m} C_{\text{col}}(\alpha_{i,j,m}) \right) \right). \quad (11)$$

The bottom section in Fig. 2 illustrates the channelization of the column attention at  $i = H$ . Later in Sect. 4.2 (Table 2 and Fig. 4), we will show with ablation experiments and visualized feature maps the impact of the channelization on improving the performance of the segmentation.

Note that, our channelized attention can also be extended to the full self-attention, which can bring a seamless mix of attention maps for all pixels. Furthermore,  $C_{\text{col}}(\alpha_{i,j,m})$  and  $C_{\text{row}}(\beta_{i,j,n})$  in Eqs. (9) and (10) can be replaced with other more powerful functions to optimize the weighted results of the spatial attention. We leave this for future work due to the page limit of this paper.

### 3.5. Grouped Vectorization

Computing self-attention row by row and column by column can save computation but it is still too slow even with parallelization. Vectorization can achieve a very high speed but it has a high requirement on GPU memory for storing the intermediate partial axial attention results  $\alpha$  (which has a dimension of  $H \times H \times W \times C$ ) and  $\beta$  (which has a dimension of  $W \times H \times W \times C$ ) in Eqs. (6) and (7). To enjoy the high speed benefit of the vectorized computation with reduced GPU memory usage, in our implementation we propose *grouped* vectorization to dynamically batch rows and columns into multiple groups, and then perform vectorization for each group respectively.

### 3.6. Going Deeper in Channel Attention

The channel attention in our method firstly uses a fully connected layer with a smaller rate to compress channels, and then uses another fully connected layer with the same

rate as the original channels, followed by a sigmoid function to generate the final channel attention weights. To further boost the performance, we explore the design of more powerful channel attention modules in channelization.

The simplest way of gaining performance is enhancing the representation ability of the neural networks, and it is usually achieved by increasing the depth and width of the networks. Here, we simply add more hidden layers before the last layer. This design allows channel attention to find better relationship between channels and find more important channels for each axial attention’s intermediate results. We also find that it is not effective to increase width, which means adding more hidden units to each layer, except for the last layer, so we keep the original settings.

Furthermore, in spatial domain, each channel of a pixel contains unique information that can lead to unique semantic representation. In our channel attention module, we find that using Leaky ReLU [20], instead of ReLU, is more effective in preventing the loss of information along deeper activations [23]. Apparently, this replacement only works in our channel attention module.

## 4. Experiments

To demonstrate the performance of our proposed CAA, comprehensive experiments are conducted with results compared with the state-of-the-art results on three benchmark datasets, *i.e.*, PASCAL Context [8], COCO-Stuff [1] and Cityscapes [19].

The same as the other existing works [9, 2, 16, 29], we measure the segmentation accuracy using mIOU (Mean Intersection Over Union). Moreover, to show the efficiency of our CAA, we also report and compare the FLOPS (Floating Point Operations per Second) of different approaches. Note that, a higher mIOU value means more accurate segmentation, whereas a lower FLOPS value indicates less computation operations. Experimental results show that our proposed CAA outperforms the state-of-the-art performance on all tested datasets in terms of mIOU.

Next, we first present the implementation details. This is followed by a series of ablation experiments conducted on the PASCAL Context dataset showing the effectiveness of each of our proposed ideas. Then, we report the comparative results obtained on PASCAL Context [8], COCO-Stuff [1] and Cityscapes [19] datasets, respectively. For fair comparison, we only compare with the methods that use ResNet-101 and naive  $8 \times$  bilinear upsampling.

### 4.1. Implementation Details

**Backbone:** Our network is built on ResNet-101 [10] pre-trained on ImageNet. The original ResNet results in a feature map of  $1/32$  of the input size. Following other similar works [4, 24, 16], we apply dilated convolution at

| Methods             | mIOU%               | FLOPS   |
|---------------------|---------------------|---------|
| ResNet-101 [10]     | -                   | 59.85G  |
| FCN [18]            | 48.12               | +0G     |
| ASPP [4]            | 50.47               | +16.7G  |
| Non-Local [25]      | 50.42               | +11.18G |
| Our Axial Attention | 50.27 ( $\pm 0.2$ ) | +8.85G  |

Table 1. Comparison results with different segmentation heads.

the output stride = 16 during training for most of the ablation experiments. We conduct experiments with the output stride = 8 during training to compare with the state of the arts.

**Segmentation Head:** We use a  $3 \times 3$  convolution to reduce the number of feature map channels from 2,048 to 512 [9, 16], which is then followed by our proposed Channelized Axial Attention module. Note that, our Axial Attention generates column attention map and row attention map from the same feature maps, instead of generating one based on the computation results of the other, as in [24]. Also, after the computation of the attention maps, we do not add the original pixel representations to the resultant feature maps. In the end, we directly upsample our logits to the input size by applying bilinear interpolation.

**Training Settings:** We employ SGD (Stochastic Gradient Descent) for optimization, where the poly decay learning rate policy  $(1 - \frac{iter}{maxiter})^{0.9}$  is applied with an initial learning rate = 0.007. We use synchronized batch normalization during training. Our experiments are conducted on  $8 \times$  TPUv3 and  $4 \times$  v100. For data augmentation, we only apply the most basic data augmentation strategies in [4] including random flip, random scale and random crop, same as in the other comparative works.

## 4.2. Experiments on Pascal Context Dataset

Pascal Context [22] dataset has 59 classes with 4,998 images for training and 5,105 images for testing. We train the network model on Pascal Context Training set with batch size = 16 with 70k iteration. During training, we set output stride = 16 and use an output stride = 8 for inference. Later in Table 4, we present our CAA results with an output stride = 16 and 8, where it can be seen clearly a 1.4% increase can be observed with the output stride = 8.

Next, we first present a series of ablation experiments conducted on the Pascal Context dataset to show the effectiveness of our proposed axial attention and channelization. Then, quantitative and qualitative comparisons with the state of the arts are presented.

**Effectiveness of Our Axial Attention.** To verify the effectiveness of our proposed Axial Attention (see Sect. 3.2), we compare the mIOU and FLOPS achieved with our Axial Attention with other segmentation heads implemented by us, as shown in Table 1. Note that our Axial Attention is different from [24], as mentioned in Sect. 3.1, and in this

| Layer Counts |   |   |   | # of Channels |     |     | mIOU%                              | FLOPS     |
|--------------|---|---|---|---------------|-----|-----|------------------------------------|-----------|
| 1            | 3 | 5 | 7 | 64            | 128 | 256 |                                    |           |
| -            | - | - | - | -             | -   | -   | 50.27( $\pm 0.2$ )                 | 68.7G     |
| ✓            |   |   |   |               | ✓   |     | 50.55( $\pm 0.2$ )                 | +0.00024G |
|              | ✓ |   |   |               | ✓   |     | 50.65( $\pm 0.2$ )                 | +0.00027G |
|              |   | ✓ |   |               | ✓   |     | <b>50.86(<math>\pm 0.2</math>)</b> | +0.00030G |
|              |   |   | ✓ |               | ✓   |     | 50.40( $\pm 0.3$ )                 | +0.00043G |
|              |   | ✓ |   | ✓             |     |     | 50.12( $\pm 0.2$ )                 | +0.00015G |
|              |   | ✓ |   |               |     | ✓   | 50.35( $\pm 0.4$ )                 | +0.00098G |

Table 2. Result comparison without using channelization (Row 1) and using channelization with different layer counts and channel numbers.

table we only compare with the methods that are independent with backbone [10]. Also, all results in this table are obtained with an output stride = 16.

From Table 1, we can easily see that our Axial Attention improves mIOU a lot compared to the Dilation-FCN (50.27 vs 48.12), which has a naive segmentation head. The mIOU obtained with our axial attention is also comparable with other approaches, such as ASPP [2, 4] and Non-Local [25]. However, our axial attention has much lower FLOPS than the original self-attention [25] (an increase of 8.85G vs 11.18G over the baseline), which demonstrates that our proposed axial attention can achieve comparable performance with the original self-attention at much lower computation cost.

**Effectiveness of Channelization.** We then use our proposed channelized dot product to replace the naive dot product in Axial Attention (see Sect. 3.4). We report the impact of adding Channelized dot product and with different depth and width in Table 2, where ‘-’ for the baseline result indicates no channelization is performed.

As it can be seen from this table, our proposed channelization improves the mIOU performance over the baseline regardless of the layer counts and the number of channels used. In particular, a best performance is achieved when the Layers = 5 and the number of Channels = 128.

**Impact of Testing Strategies.** We report and compare the performance and computation cost of our proposed model against the baseline and the DANet with different testing strategies. This is shown in Table 3. Same as the settings in other works [32, 9], we add multi-scale, left-right flip and aux loss [32, 9] during inference. Note that, in this table, we report the mean mIOU figures with a dynamic range to show the stability of our algorithm.

**Comparison with the State of the Arts.** Finally, we compare our proposed approach with the state-of-the-art approaches. The results on the Pascal Context dataset is shown in Table 4. Like other similar works, we apply multi-scale and left-right flip during inference. For fair comparison, we only compare with the methods that use ResNet-101 and naive decoder (directly upsampling logits). Also note that, in this and the following tables, we report the best

| Methods            | Train OS    |        | Eval OS |             | Strategies<br>MS flip | Aux Loss         | mIOU%  | FLOPs                       |
|--------------------|-------------|--------|---------|-------------|-----------------------|------------------|--|-----------------------------|
|                    | 16          | 8      | 16      | 8           |                       |                  |  |                             |
| ResNet-101 [10]    | -           | -      | ✓       | ✓           |                       | -                | -  | 59.85G<br>190.70G           |
| DANet [9]          |             | ✓<br>✓ |         | ✓<br>✓      | ✓ ✓                   | -<br>✓           | -<br>52.60   | +101.25G<br>-               |
| Our CAA            | ✓<br>✓<br>✓ |        | ✓       | ✓<br>✓      |                       |                  | 50.86(±0.2)<br>51.36(±0.2)<br>53.02(±0.3)                | +8.85G<br>+34.33G<br>-      |
| Our CAA + Aux loss | ✓<br>✓<br>✓ |        | ✓       | ✓<br>✓<br>✓ | ✓ ✓                   | ✓<br>✓<br>✓<br>✓ | 51.43(±0.2)<br>52.02(±0.2)<br>53.48(±0.2)<br>54.51(±0.4) | +8.85G<br>+34.33G<br>-<br>- |

Table 3. Comparison results with different testing strategies. **Train OS**: Output stride in training. **Eval OS**: Output stride in inference. **MS**: Apply multi-scale during inference. **Aux loss**: Add auxiliary loss during training. “+” refers to the FLOPS over the baseline FLOPS of ResNet-101.

| Methods                       | mIOU%       | Ref      |
|-------------------------------|-------------|----------|
| FCN [18]                      | 50.8        | CVPR2015 |
| ENet [30]                     | 51.7        | CVPR2018 |
| DeepLab [4]                   | 52.7        | ECCV2018 |
| ANet [34]                     | 52.8        | ICCV2019 |
| EMANet [16]                   | 53.1        | ICCV2019 |
| SVCNet [7]                    | 53.2        | CVPR2019 |
| SPYGR [15]                    | 52.8        | CVPR2020 |
| CPN [28]                      | 53.9        | CVPR2020 |
| CFNet [31]                    | 54.0        | CVPR2019 |
| DANet [9]                     | 52.6        | CVPR2019 |
| Our CAA (OS = 16 Train)       | 53.6        | -        |
| <b>Our CAA (OS = 8 Train)</b> | <b>54.9</b> | -        |

Table 4. Result comparison with the state-of-the-art approaches on the Pascal Context testing set for multi-scale prediction.

results of our approach obtained in experiments.

As shown in this table, our proposed CAA method achieves the highest score in the methods trained with an output stride = 16 with ResNet-101 and naive decoder, and even outperforms some methods trained with an output stride = 8. Moreover, after we train our model with an output stride = 8, the performance of our model has been further improved and outperforms all of the state-of-the-art models, including the ones recently published in CVPR2019 and CVPR2020.

In Fig. 3, we provide the visualizations of the prediction results obtained with our CAA model in comparison with the state-of-the-art approaches. As shown in the figure, our model is able to segment objects very well without requiring any post-processing.

To further demonstrate the effectiveness of our proposed channelization, in Fig. 4 we visualize the feature maps obtained after applying the column attention and row attention maps and the difference between the corresponding feature maps with and without applying the channel attentions.

### 4.3. Results on COCO-Stuff 10K Dataset

Following the other works [16, 29, 9], we demonstrate that our model can handle complex images with a large

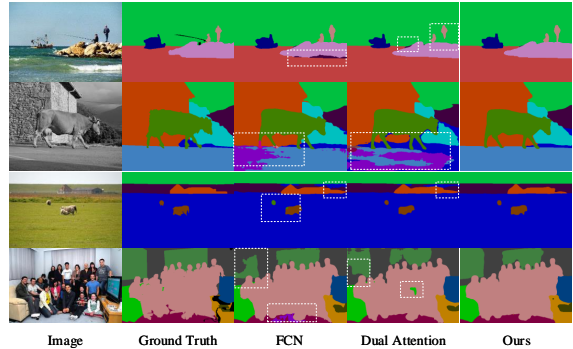


Figure 3. The visualization of the prediction results on the Pascal Context dataset [22] obtained with our proposed CAA in comparison with the results obtained with FCN [18], DANet [9] and the ground truth. All results are inferred with an output stride = 8.

| Methods        | mIOU%       | Ref      |
|----------------|-------------|----------|
| DSSPN [17]     | 38.9        | CVPR2018 |
| SVCNet [7]     | 39.6        | CVPR2019 |
| EMANet [16]    | 39.9        | ICCV2019 |
| SPYGR [15]     | 39.9        | CVPR2020 |
| OCR [29]       | 39.5        | ECCV2020 |
| DANet [9]      | 39.7        | CVPR2019 |
| <b>Our CAA</b> | <b>41.2</b> | -        |

Table 5. Comparison results with other approaches on the COCO-Stuff 10K testing set for multi-scale prediction.

number of classes. We further evaluate our model on the COCO-Stuff 10K dataset [1], which contains 9,000 training images and 1,000 testing images, as shown in Table 5. As it can be seen from the table, our proposed CAA outperforms all other state-of-the-art approaches by a large margin of 1.3%.

### 4.4. Results on Cityscapes Dataset

The Cityscapes dataset [19] has 19 classes. Its *fine* set contains high quality pixel-level annotations of 5,000 images, where there are 2,975, 500 and 1,525 images in the

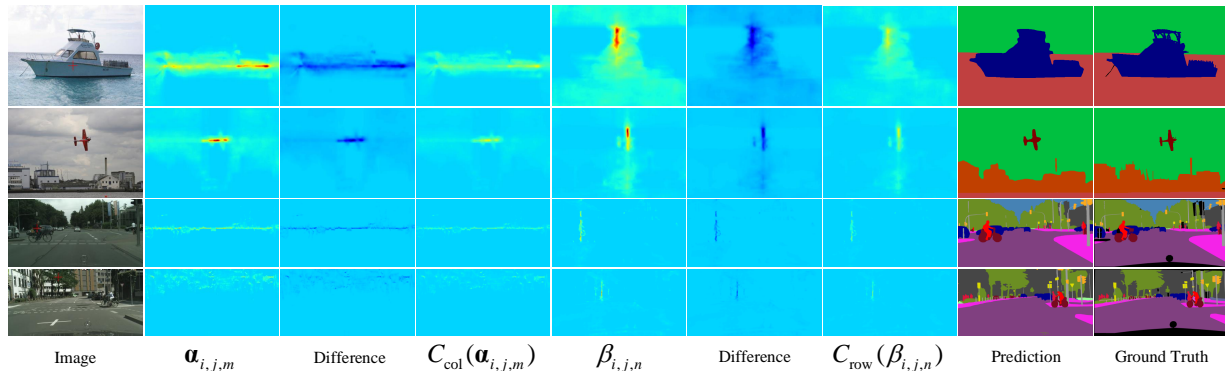


Figure 4. Visualization of the feature maps ( $\alpha_{i,j,m}$ ,  $C_{\text{col}}(\alpha_{i,j,m})$ ,  $\beta_{i,j,n}$  and  $C_{\text{row}}(\beta_{i,j,n})$ ) on Pascal Context [22] (top two rows) and Cityscapes [19] (bottom two rows). For each input image, we list the feature maps obtained after applying the column attention map and row attention map, the difference between the corresponding feature maps with and without applying the channel attentions, as well as our prediction and the ground truth segmentation, respectively. For more details, please refer to Sect. 2.

| Methods        | mIOU%       | Ref      |
|----------------|-------------|----------|
| PSPNet [32]    | 78.4        | CVPR2017 |
| CFNet [31]     | 79.6        | CVPR2019 |
| ANNN [34]      | 81.3        | ICCV2019 |
| CCNet [13]     | 81.4        | ICCV2019 |
| CPN [28]       | 81.3        | CVPR2020 |
| SPYGR [15]     | 81.6        | CVPR2020 |
| OCR [29]       | 81.8        | ECCV2020 |
| DANet [9]      | 81.5        | CVPR2019 |
| <b>Our CAA</b> | <b>82.6</b> | -        |

Table 6. Comparison results with other state-of-the-art approaches on the Cityscapes Test set for multi-scale prediction.

Training, Validation, and Test sets, respectively. Like other works [15, 9], we crop the training images to  $769 \times 769$  during training, and keep full-resolution  $1025 \times 2049$  during inference. We report our results<sup>2</sup> in Table 6 and also visualize our feature maps and results in Fig. 4 (the bottom two rows).

#### 4.5. Effectiveness of Grouped Vectorization

In Sect. 3.5, we developed the grouped vectorization to split tensors into multiple groups so as to reduce the GPU memory usage when performing channel attention in Eqs. (9) and (10). The more groups used in group vectorization, the proportionally less GPU memory is needed for the computation, yet with longer inference time. In this section, we conduct experiments to show the variation of the inference time (seconds/image) when different numbers of groups are used in group vectorization.

Fig. 5 shows the results where three different input resolutions are tested. As shown in this graph, when splitting the vectorization into smaller numbers of groups, e.g., 2 or 4, our grouped vectorization can achieve comparable inference speed with one half or one quarter of the original spa-

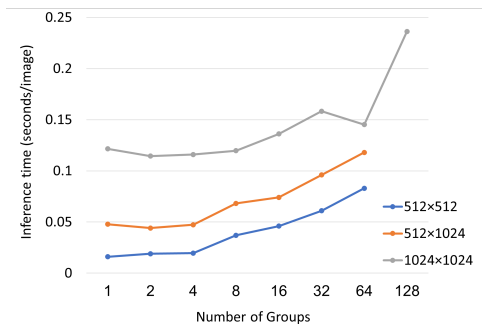


Figure 5. Inference time (seconds/image) when applying different numbers of groups in grouped vectorization.

cial complexity.

## 5. Conclusion

In this paper, aiming to combine the advantages of the popular self-attention and channel attention, we have proposed a novel and effective Channelized Axial Attention approach for semantic segmentation. After computing column and row attentions, we proposed to capture the intermediate results and perform the corresponding channel attention on each of them. Our proposed approach of applying the column and row attentions transpositionally has allowed the channelization to be conducted in the whole respective field. Experiments on the three popular benchmark datasets have demonstrated the superiority and effectiveness of our proposed axial attention and channelization in terms of both segmentation performance and computational complexity.

## References

- [1] Holger Caesar, Jasper Uijlings, and Vittorio Ferrari. Coco-stuff: Thing and stuff classes in context. In *Conference on Computer Vision and Pattern Recognition*, 2018. 2, 5, 7

<sup>2</sup><https://www.cityscapes-dataset.com/anonymous-results/?id=86b37...>



- [2] Liang-Chieh Chen, George Papandreou, Iasonas Kokkinos, Kevin Murphy, and Alan L Yuille. Deeplab: Semantic image segmentation with deep convolutional nets, atrous convolution, and fully connected crfs. *IEEE Transactions on Pattern Analysis and Machine Intelligence*, 2017. 1, 2, 5, 6
- [3] Liang-Chieh Chen, George Papandreou, Florian Schroff, and Hartwig Adam. Rethinking atrous convolution for semantic image segmentation, 2017. 1
- [4] Liang-Chieh Chen, Yukun Zhu, George Papandreou, Florian Schroff, and Hartwig Adam. Encoder-decoder with atrous separable convolution for semantic image segmentation. In *European Conference on Computer Vision*, 2018. 1, 2, 5, 6, 7, 11
- [5] Yunpeng Chen, Yannis Kalantidis, Jianshu Li, Shuicheng Yan, and Jiashi Feng. A2-nets: Double attention networks. In *Conference on Neural Information Processing Systems*, 2018. 2
- [6] Francois Chollet. Xception: Deep learning with depthwise separable convolutions. In *Conference on Computer Vision and Pattern Recognition*, 2017. 11
- [7] Henghui Ding, Xudong Jiang, Bing Shuai, Ai Qun Liu, and Gang Wang. Semantic correlation promoted shape-variant context for segmentation. In *Conference on Computer Vision and Pattern Recognition*, 2019. 7
- [8] Mark Everingham, Luc Van Gool, Christopher K.I. Williams, John Winn, and Andrew Zisserman. The pascal visual object classes (voc) challenge. *International Journal of Computer Vision*, 2009. 2, 5
- [9] Jun Fu, Jing Liu, Haijie Tian, Yong Li, Yongjun Bao, Zhe-wei Fang, and Hanqing Lu. Dual attention network for scene segmentation. In *Conference on Computer Vision and Pattern Recognition*, 2019. 1, 2, 3, 5, 6, 7, 8, 11
- [10] Kaiming He, Xiangyu Zhang, Shaoqing Ren, and Jian Sun. Deep residual learning for image recognition. In *Conference on Computer Vision and Pattern Recognition*, 2016. 3, 5, 6, 7, 11
- [11] Jonathan Ho, Nal Kalchbrenner, Dirk Weissenborn, and Tim Salimans. Axial attention in multidimensional transformers, 2019. 2, 3
- [12] Jie Hu, Li Shen, and Gang Sun. Squeeze-and-excitation networks. In *Conference on Computer Vision and Pattern Recognition*, 2018. 1, 2
- [13] Zilong Huang, Xinggang Wang, Yunchao Wei, Lichao Huang, Humphrey Shi, Wenyu Liu, and Thomas S. Huang. Ccnet: Criss-cross attention for semantic segmentation. *IEEE Transactions on Pattern Analysis and Machine Intelligence*, 2020. 2, 8, 11
- [14] Alexander Kirillov, Kaiming He, Ross Girshick, Carsten Rother, and Piotr Dollar. Panoptic segmentation. In *Conference on Computer Vision and Pattern Recognition*, 2019. 11
- [15] Xia Li, Yibo Yang, Qijie Zhao, Tiancheng Shen, Zhouchen Lin, and Hong Liu. Spatial pyramid based graph reasoning for semantic segmentation. In *Conference on Computer Vision and Pattern Recognition*, 2020. 7, 8
- [16] Xia Li, Zhisheng Zhong, Jianlong Wu, Yibo Yang, Zhouchen Lin, and Hong Liu. Expectation-maximization attention networks for semantic segmentation. In *International Conference on Computer Vision*, 2019. 1, 5, 6, 7, 11
- [17] Xiaodan Liang, Hongfei Zhou, and Eric Xing. Dynamic-structured semantic propagation network. In *Conference on Computer Vision and Pattern Recognition*, 2018. 7
- [18] Jonathan Long, Evan Shelhamer, and Trevor Darrell. Fully convolutional networks for semantic segmentation. In *Conference on Computer Vision and Pattern Recognition*, pages 3431–3440, 2015. 1, 6, 7
- [19] Cordts Marius, Omran Mohamed, Ramos Sebastian, Rehfeld Timo, Enzweiler Markus, Benenson Rodrigo, Franke Uwe, Stefan Roth, and Schiele Bernt. The cityscapes dataset for semantic urban scene understanding. In *Conference on Computer Vision and Pattern Recognition*, 2016. 2, 5, 7, 8, 11
- [20] Andrew L. Mass, Awni Y. Hannun, and Andrew Y. Ng. Rectifier nonlinearities improve neural network acoustic models. In *International Conference on Machine Learning*, 2013. 5
- [21] Tan Mingxing and Le Quoc. Efficientnet: Rethinking model scaling for convolutional neural networks. In *International Conference on Machine Learning*, 2019. 11
- [22] Roozbeh Mottaghi, Xianjie Chen, Xiaobai Liu, Nam-Gyu Cho, Seong-Whan Lee, Sanja Fidler, Raquel Urtasun, and Alan Yuille. The role of context for object detection and semantic segmentation in the wild. In *Conference on Computer Vision and Pattern Recognition*, 2014. 6, 7, 8
- [23] Mark Sandler, Andrew Howard, Menglong Zhu, Andrey Zhmoginov, and Liang-Chieh Chen. Mobilenetv2: Inverted residuals and linear bottlenecks. In *Conference on Computer Vision and Pattern Recognition*, 2018. 5
- [24] Huiyu Wang, Yukun Zhu, Bradley Green, Hartwig Adam, Alan Yuille, and Liang-Chieh Chen. Axial-deeplab: Stand-alone axial-attention for panoptic segmentation. In *European Conference on Computer Vision*, 2020. 3, 4, 5, 6, 11
- [25] Xiaolong Wang, Ross Girshick, Abhinav Gupta, and Kaiming He. Non-local neural networks. In *Conference on Computer Vision and Pattern Recognition*, 2018. 1, 2, 3, 6
- [26] Sanghyun Woo, Jongchan Park, Joon-Young Lee, and So Kweon. Convolutional block attention module. In *European Conference on Computer Vision*, 2018. 2
- [27] Maoke Yang, Kun Yu, Chi Zhang, Zhiwei Li, and Kuiyuan Yang. Denseaspp for semantic segmentation in street scenes. In *Conference on Computer Vision and Pattern Recognition*, 2018. 1, 2, 11
- [28] Changqian Yu, Jingbo Wang, Changxin Gao, Gang Yu, Chunhua Shen, and Nong Sang. Context prior for scene segmentation. In *Conference on Computer Vision and Pattern Recognition*, 2020. 7, 8
- [29] Yuhui Yuan, Xilin Chen, and Jingdong Wang. Object-contextual representations for semantic segmentation. In *European Conference on Computer Vision*, 2020. 1, 5, 7, 8, 11
- [30] Hang Zhang, Kristin Dana, Jianping Shi, Zhongyue Zhang, Xiaogang Wang, Amrith Tyagi, and Amit Agrawal. Context encoding for semantic segmentation. In *Conference on Computer Vision and Pattern Recognition*, 2018. 7, 11
- [31] Hang Zhang, Han Zhan, Chenguang Wang, and Junyuan Xie. Semantic correlation promoted shape-variant context for segmentation. In *Conference on Computer Vision and Pattern Recognition*, 2019. 7, 8, 11

- [32] Hengshuang Zhao, Jianping Shi, Xiaojuan Qi, Xiaogang Wang, and Jiaya Jia. Pyramid scene parsing network. In *Conference on Computer Vision and Pattern Recognition*, 2017. [1](#), [2](#), [6](#), [8](#), [11](#)
- [33] Zilong Zhong, Zhong Qiu Lin, Rene Bidart, Xiaodan Hu, Ibrahim Ben Daya, and Zhifeng Li. Squeeze-and-attention networks for semantic segmentation. In *Conference on Computer Vision and Pattern Recognition*, 2020. [11](#)
- [34] Zhen Zhu, Mengde Xu, Song Bai, Tengting Huang, and Xiang Bai. Asymmetric non-local neural networks for semantic segmentation. In *International Conference on Computer Vision*, 2019. [2](#), [7](#), [8](#), [11](#)

| Attention Base  | Eval OS | Channelized | Aux loss | mIOU% |
|-----------------|---------|-------------|----------|-------|
| Axial Attention | 16      |             |          | 50.27 |
|                 | 16      | ✓           |          | 50.86 |
|                 | 16      | ✓           | ✓        | 51.43 |
| Self Attention  | 16      |             |          | 50.42 |
|                 | 16      | ✓           |          | 50.79 |
|                 | 16      | ✓           | ✓        | 50.90 |

Table 7. Ablation study of applying our Channelized Attention on self-attention with ResNet-101 [10]. **Eval OS**: Output strides [4] during evaluation. **Aux loss**: Add auxiliary loss during training.

## 6. Appendix

### 6.1. Channelized Self-Attention

In our main paper, we proposed the Channelized Axial Attention (CAA) approach and applied channelization to our axial attention, which has achieved the state-of-the-art performance in multiple datasets. In this section, we conduct additional experiments on the Pascal Context testing set by applying channelization to the original self-attention. We report its single-scale performance in Table 7 with ResNet-101 [10].

We can see from the table that our proposed channelized method can further improve the performance of self-attention slightly by 0.37% and 0.48% without and with auxiliary loss. It also shows the current channelized design is more effective for our Axial Attention (0.59% vs 0.37%). However, slightly adjusting the design of our channel attention may help to further boost the performance of channelized self-attention. We leave this for future work.

### 6.2. Alternative Backbones

In our main paper, we have reported our CAA’s performance using ResNet-101 [10] as backbone, which is widely used in semantic segmentation [4, 9, 13, 16, 27, 29, 30, 31, 32, 33, 34]. In this Section, we conduct additional experiments on Pascal Context by attaching our CAA module with some other backbones. We report our results obtained with single scale without flipping in Table 8.

Table 8 shows that both our Axial Attention and Channelization approaches have improved the mIOU of the baseline in multiple well-know backbones. We also find that our Channelization approach is more effective with ResNet and EfficientNet, whereas the improvement on Xception65 is relatively small.

### 6.3. Comparison with Axial-DeepLab

In our main paper, we mentioned that our proposed Axial Attention has much difference with the Axial-DeepLab [24]. It is very hard to compare our approach with Axial-DeepLab fairly since Axial-DeepLab is embedded in multiple places of the original ResNet, resulting a new backbone named “Axial-ResNet”. Also note

| Backbone            | Eval OS | Axial Attention | Channelized | mIOU% |
|---------------------|---------|-----------------|-------------|-------|
| ResNet-50 [10]      | 16      |                 |             | 46.92 |
|                     | 16      | ✓               |             | 49.73 |
|                     | 16      | ✓               | ✓           | 50.23 |
| ResNet-101 [10]     | 16      |                 |             | 48.12 |
|                     | 16      | ✓               |             | 50.27 |
|                     | 16      | ✓               | ✓           | 50.86 |
| Xception65 [6, 4]   | 16      |                 |             | 49.40 |
|                     | 16      | ✓               |             | 52.42 |
|                     | 16      | ✓               | ✓           | 52.65 |
| EfficientNetB7 [21] | 16      |                 |             | 52.35 |
|                     | 16      | ✓               |             | 52.84 |
|                     | 16      | ✓               | ✓           | 53.90 |
|                     | 8       | ✓               | ✓           | 55.12 |

Table 8. Ablation study of applying our Channelized Axial Attention to other backbones. All results are obtained in single scale without flipping. **Axial Attention**: Using our Axial Attention after backbone. **Channelized**: Applying our Channelized approach. **Eval OS**: Output strides [4] during evaluation.

| Method           | Backbone             | Cityscapes Fine | mIOU% |
|------------------|----------------------|-----------------|-------|
| Axial-DeepLab-L  | Axial-ResNet-L [24]  | ✓               | 79.5  |
| Axial-DeepLab-XL | Axial-ResNet-XL [24] | ✓               | 79.9  |
| Our CAA          | ResNet-101[10]       | ✓               | 82.6  |

Table 9. Comparison of our CAA with Axial-DeepLab [24]. **Cityscapes Fine**: the model is trained with Cityscapes Fine set only.

that, Axial-DeepLab was designed for panoptic segmentation [14]. In this section, we compare the semantic segmentation results obtained with our CAA and Axial-DeepLab in Cityscapes [19] dataset to give readers a new perspective of the effectiveness of our CAA. This is shown in Table 9.